



Finite Element Simulation of Temperature and Strain Distribution during Friction Stir Welding of AA2024 Aluminum Alloy

Rahul Jain¹ · Surjya Kanta Pal¹ · Shiv Brat Singh²

Received: 8 September 2015 / Accepted: 19 May 2016 / Published online: 20 June 2016
© The Institution of Engineers (India) 2016

Abstract Friction Stir Welding (FSW) is a solid state joining process and is handy for welding aluminum alloys. Finite Element Method (FEM) is an important tool to predict state variables of the process but numerical simulation of FSW is highly complex due to non-linear contact interactions between tool and work piece and interdependency of displacement and temperature. In the present work, a three dimensional coupled thermo-mechanical method based on Lagrangian implicit method is proposed to study the thermal history, strain distribution and thermo-mechanical process in butt welding of Aluminum alloy 2024 using DEFORM-3D software. Workpiece is defined as rigid-visco plastic material and sticking condition between tool and work piece is defined. Adaptive remeshing is used to tackle high mesh distortion. Effect of tool rotational and welding speed on plastic strain is studied and insight is given on asymmetric nature of FSW process. Temperature distribution on the workpiece and tool is predicted and maximum temperature is found in workpiece top surface.

Keywords Friction stir welding · Finite element method · Temperature distribution

Introduction

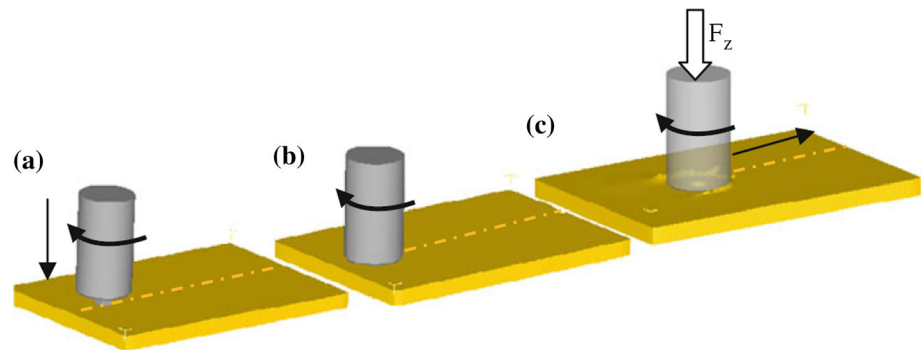
Friction Stir Welding (FSW) is a solid state joining process invented by TWI England [1]. In FSW, the temperature of the material remains below the solidus temperature and hence the defects associated with solidification of the material are eliminated. Also, in FSW, a non-consumable rotating tool is plunged into the work piece to generate heat due to friction at the interference and plastic deformation of the material. This heat plasticizes the material and brings it into a viscous state; and then the tool travels along the welding line to stir the material along the welding direction. Schematic representation of different stages of the FSW process is shown in Fig. 1. Heat generation between rotating tool and work-piece is responsible for plasticizing and softening of the material, and this softened material is subjected to extrusion by traverse speed and tool pin rotation which leads to formation of weld nugget zone [2, 3]. Simulation of FSW process is complex due to highly non linear contact interaction between tool and work piece, unknown boundary conditions and material flow behavior during welding. Nevertheless, over the last few years finite element analysis of FSW is under the radar of several researchers. Some investigators [4] have simulated the FSW process as two different boundary value problems, first is the steady state heat transfer to the tool and second is transient heat transfer analysis of the workpiece. They have considered workpiece as a symmetric body and only frictional heat had been considered. They found that 95 % of the generated heat goes to the workpiece and only 5 % of the heat goes to the tool. It has also been [5] modeled the FSW by considering symmetry of the process along the weld line and developed a heat flux equation by measuring the

✉ Rahul Jain
rahuljain214@gmail.com

¹ Department of Mechanical Engineering, Indian Institute of Technology, Kharagpur, India

² Department of Metallurgical and Materials Engineering, Indian Institute of Technology, Kharagpur, India

Fig. 1 Schematic representation of sequence of FSW process **a** First stage: plunging, **b** Second stage: Dwelling, **c** Third stage: Welding. *Dashed line* indicates abutting edges, while *arrows* indicates the direction of tool movement [3]



temperature in FSW through experiment by earlier researchers. They have not considered material deformation during the simulation and only sliding friction has been considered. The researchers [6] have performed a three dimensional Finite Element Analysis (FEA) of thermal history in FSW by using Johnson–Cook material and damage models in ABAQUS/Explicit. Because of damage model, mesh near the pin was deleted and the simulation did not have any weld nugget zone. They have also studied the plunging and dwelling periods in FSW. Effect of heat transfer from the backing plate on temperature distribution was also considered. Some investigators [7] have developed a mathematical equation for heat generation and validated it by measuring power through experiments. They have considered heat generation through friction (both sticking and sliding friction) only, but neglected the heat generation by mechanical deformation. The researchers have [8, 9] have developed a 3D visco-plastic model of FSW to estimate temperature history and material flow and validated the same with experimental data. They have assumed the material as a non-Newtonian fluid and allowed the flow stress to vary as a function of temperature and strain rate. Some of the investigators [10, 11] have done a 3D analysis of FSW in DEFROM 3D to predict temperature history and strain profile during welding. They have used the flow stress as a function of temperature, strain and strain rate. Regression analysis was used to calculate material constants. The researchers [12] have developed a fully coupled 3D analysis to estimate temperature and strain profiles. Material flow is also simulated for different time intervals of the simulation. They have used arbitrary Lagrangian and Eulerian analyses to simulate FSW in ABAQUS/Explicit. Simple coulomb law of friction was considered for the analysis. Some investigators have [13] have used the solid mechanics approach to model FSW for welding magnesium alloy. They have simulated the thermal history. Similarly, a number of researchers have also developed mathematical expression for heat generation in FSW due to friction either by assuming constant

contact pressure or neglecting heat generation due to mechanical deformation of work piece or by simplifying the contact by using Coulomb's law of friction. Also, FSW is simulated by considering symmetry along the weld line which is not true in practical situation. The researchers [14] have considered two different frictional boundary conditions i.e. Norton and Coulomb's friction law to calibrate the steady state welding forces and tool temperatures at different location. They claim that frictional boundary condition is important for the accurate modeling of the process. The model is based on ALE method. It has been [15] developed earlier by the several researchers a 3D thermo-mechanical model based on lagrangian technique. They have predicted the temperature and strain evolution that can be used for prediction of stirred zone. They have used point tracking method to predict material flow and found out that major material flow takes place from the advancing side of the weld, which lead to higher strain on the advancing side as compared to the retreating side. The researchers [16] have used coupled Eulerian–Lagrangian method to simulate FSW process. They have used Johnson–Cook material model to define flow stress. They have validated the model with the axial force and torque during plunging phase of the process.

Weld-line symmetry, uncoupled analysis are some of the major assumptions considered by the researchers. In few cases, only steady state welding is considered and plunging phase is neglected. In the present paper to simulate the FSW process from initial to steady state a 3D coupled temperature-displacement analysis is used to simulate FSW process with Lagrangian incremental technique. Adaptive remeshing is used to take care of mesh integrity. Model is capable of predicting strain and temperature distribution and its variation with rotational speed. It's a proven fact that FSW is an asymmetric process due to variation in relative velocity in advancing and re-treating side. Model predicts the similar nature of the process with the help of strain distribution across the transverse direction of the weld.

Model Description

Geometric Modeling

A 3D analysis of FSW is performed in DEFORM-3D. Lagrangian implicit code is used along with adaptive re-meshing technique. Fully coupled temperature-displacement analysis is considered i.e. at every time increment, temperature and displacement are calculated at each node simultaneously. AA2024 aluminum alloy is taken as the work piece and is modeled as rigid visco-plastic material. Dimension of work piece is 80 mm × 60 mm × 5 mm. Work piece is meshed with 10,339 nodes, which forms 44,730 tetrahedral elements. Tool steel H13 is used as the tool material which is modeled as a rigid body i.e. stress and strain are not calculated on tool but heat transfer from work piece is considered. Since, the yield stress of tool steel is much higher than aluminum alloy, considering rigid tool is a valid assumption. Tool is meshed with 9181 nodes, which form 40,247 tetrahedral elements. Shoulder diameter of tool is 24 mm. Tapered cylindrical pin is used with larger diameter of 7 mm with included angle of 40° and pin height of 4.6 mm. Tool and work piece meshing is shown in Fig. 2. Mesh window is used to refine the mesh at the contact region to have better result and this refined mesh will follow the tool during tool traverse movement. Boundary conditions assigned to FSW model are bottom surface of work piece is fixed by assigning zero velocity, with this all movements of work piece is restricted. Rotational (Z-direction) and transverse (X-direction) velocities are assigned to the tool.

Convective heat transfer coefficient of 20 W/m²/°C [15] is defined between work piece-environment and tool-environment to accommodate heat transfer between them. Conductive heat transfer takes place from bottom face of workpiece to the backing plate during welding. Here,

conductive heat transfer is equated with convective heat transfer as mentioned in Eq. 1, and convective heat transfer coefficient between bottom surface of work piece and environment is defined as, 200 W/m²/°C. This assumption makes the model computationally efficient, as backing plate is no more required to be modeled.

$$k \frac{\partial T}{\partial z} = h \Delta T \tag{1}$$

where, k is thermal conductivity, h is convective heat transfer coefficient, T is temperature.

Finite element formulation

A rigid visco-plastic model with von-mises yield criteria is used. FSW is a large deformation process where, the plastic strain is much greater than elastic strain. Therefore, elastic strain can be neglected and hence, consideration of visco-plastic model is justified. Following stress–strain rate relations are used in deformation zone,

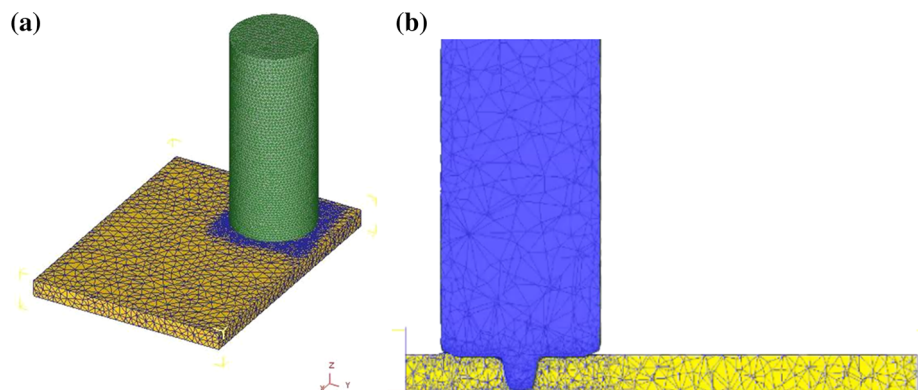
$$\dot{\epsilon}_{ij} = \frac{3}{2} \frac{\dot{\bar{\epsilon}}}{\bar{\sigma}} \sigma'_{ij} \tag{2}$$

$$\bar{\sigma} = \sqrt{\frac{3}{2} \sigma'_{ij} \sigma'_{ij}} \tag{3}$$

$$\dot{\bar{\epsilon}} = \sqrt{\frac{2}{3} \dot{\epsilon}_{ij} \dot{\epsilon}_{ij}} \tag{4}$$

where, $\bar{\sigma}$, $\dot{\bar{\epsilon}}$, $\dot{\epsilon}_{ij}$, σ'_{ij} are effective stress/flow stress, effective strain rate, strain rate components and deviatoric stress components respectively. Finite element formulation of rigid visco-plastic material is based on the variational approach in which the admissible velocities, u_i should satisfy the conditions of compatibility and incompressibility, and also the velocity boundary conditions, which give the following functional (function of a function) a stationary value,

Fig. 2 Meshing of workpiece and tool **a** Isometric view, **b** X–Z plane



$$\pi = \int_V E(\dot{\varepsilon}_{ij})dV - \int_{S_F} F_i u_i dS \quad (5)$$

where, F_i , V , S_F , and $E(\dot{\varepsilon}_{ij})$ are surface tractions, volume of the workpiece, force surface and work function respectively. A penalized form of the incompressibility is added to remove the incompressibility constraint on admissible velocity fields. The actual velocity field can now be determined from the stationary value of the variation equation, which is stated as,

$$\delta\pi = \int_V \bar{\sigma} \delta\dot{\varepsilon} dV + \lambda \int_V \dot{\varepsilon}_v \delta\dot{\varepsilon}_v dV - \int_{S_F} F_i \delta u_i dS = 0 \quad (6)$$

where, λ and δu_i are large penalty constant and arbitrary variation respectively. $\delta\dot{\varepsilon}$ and $\delta\dot{\varepsilon}_v$ are variations in strain rate derived from $\delta u_i \cdot \dot{\varepsilon}_v = \dot{\varepsilon}_{ii}$ is the volumetric strain rate [17].

Material Model

Appropriate choice of material model is vital for accurate solution during simulation. Material undergoes from solid to viscous state; therefore it is necessary to define flow stress value for a wide range of strain, strain rate and temperature. Flow stress is defined as a function of strain, strain rate, temperature, as given in Eq. 7. Therefore, to define flow stress, stress–strain behavior at different strain rates (0.3–100/s) and temperatures (20–550 °C) from DEFORM material library is used as input to the simulation, and isotropic hardening rule is considered.

$$\bar{\sigma} = \bar{\sigma}(\varepsilon, \dot{\varepsilon}, T) \quad (7)$$

where, $\bar{\sigma}$ is flow stress, ε is strain, $\dot{\varepsilon}$ is strain rate, T is temperature.

Thermal Model

In FSW, heat is generated due to friction and plastic deformation of the material as mentioned in Eq. 8. In DEFORM 3D inelastic heat fraction is defined to incorporate heat generated due to plastic deformation, as given in Eq. 9.

$$\dot{q} = \dot{q}_f + \dot{q}_p \quad (8)$$

where, \dot{q} is the heat generation during the process, \dot{q}_f is the frictional heat generation, \dot{q}_p is the heat generated due to plastic deformation of the material.

$$\dot{q}_p = \eta \bar{\sigma} \times \dot{\varepsilon} \quad (9)$$

where, η is inelastic heat fraction or amount of mechanical work converted to heat energy and it is taken as 0.9 [10] in

Table 1 Physical properties of material (from DEFORM manual)

Properties	AA2024	Tool steel H13
Young's modulus, N/mm ²	68,900	210,000
Thermal conductivity, N/s °C	181	149
Heat capacity, N/mm ² °C	2.43	2.78
Thermal expansion, μmm/mm °C	22	11.7
Poisson's ratio	0.33	0.3

this work. Temperature distribution is dictated by Fourier law of heat conduction equation, as stated in Eq. 10.

$$k\nabla^2 T + \dot{q} = \rho c_p \frac{\partial T}{\partial t} \quad (10)$$

where, k is thermal conductivity of the material, T is temperature in °C, ρ is density of the material, and c_p is the heat capacity of the material per unit mass. Transient heat transfer analysis is considered in this work.

Frictional Model

Contact conditions between the tool and the workpiece in FSW is very complex and due to lack of experimental data and evidence of actual condition, the researchers have assumed different contact conditions. Some researchers have assumed coulomb's law of friction [12, 14]; whereas some others have assumed sticking condition [10, 15]. A few researchers [8, 9, 18] have used a friction model, which is a function of pressure and slip rate. In the present work, sticking boundary condition, as given in Eq. 2, is used. This consideration is used because of the fact that yield strength of the material is the limiting condition of contact stress at the interface.

$$\bar{\tau} = m\tau_{\max} \quad (11)$$

where, $\bar{\tau}$ is contact stress in MPa at the interface of the tool and the work piece, m is shear factor, whose value is 1, τ_{\max} is the shear yield strength of the material which is 0.577 times of the yield strength of the material according to von-Mises yield criteria. Table 1 show the various mechanical and thermal property used during the simulation.

Results and Discussions

Temperature Profile

In FSW, certain amount of heat is required to plasticize the material, which allows mixing of material to achieve a good weld. Heat is generated in FSW due to plastic deformation of material and frictional heat generated

Fig. 3 Temperature profile in longitudinal direction and top surface of work piece (for 1000 rpm, and 60 mm/min traverse speed)

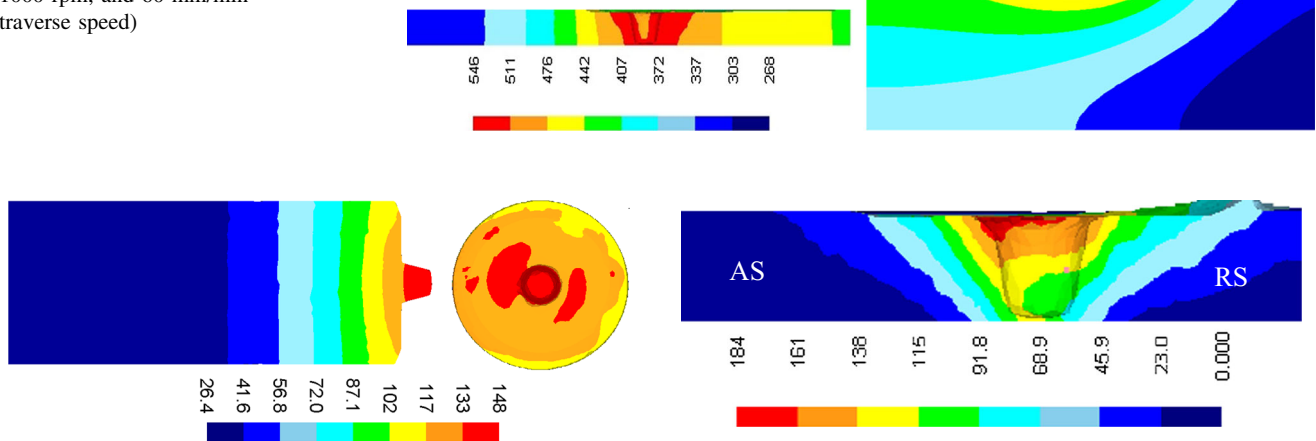


Fig. 4 Temperature distribution on FSW tool for rotational speed of 1000 rpm and 60 mm/min

between tool and work piece. The latter depends on shear friction factor and contact area. Figure 3 shows the calculated temperature distribution along the weld line and top surface of the work piece. Maximum temperature is obtained at the centre of the weld because rotation of the shoulder and probe which contributes towards the highest heat generation in this region. Moreover, the temperature profile along the thickness attains a ‘V’ shape; this is because shoulder larger diameter as compared to the pin, which leads to larger heat generation on top surface as compared to the bottom and also, convection heat transfer between bottom of work piece and backing plate is much higher (high convective heat transfer coefficient due to contact pressure between them) than convection heat transfer between top of work piece and atmosphere. This difference of convective heat transfer coefficient leads to higher cooling at the bottom of work piece and formation of V shaped temperature profile.

Tool temperature distribution is important for selection of the tool material. Tool material should be chosen such that it should have the required strength and hot hardness. Figure 4 shows the temperature distribution on the FSW tool. Maximum temperature is obtained as 148 °C on the

Table 2 Validation of simulation results with experimental data

Rotational speed, rpm	Maximum temperature during FSW process		Percentage error, %
	Experimental [19], °C	Simulation, °C	
350	257	243.7	5.4
950	349	358.61	2.7

Fig. 5 Strain, mm/mm profile along y–z section for 1000 rpm and 60 mm/min

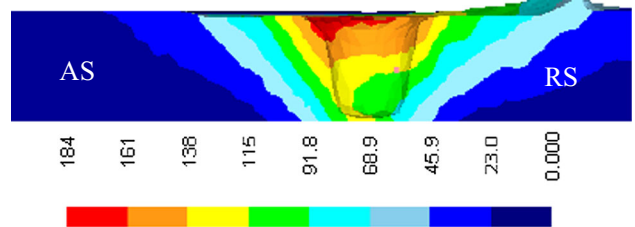
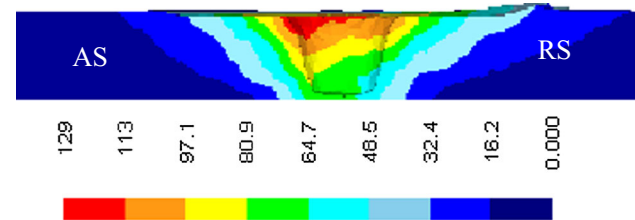


Fig. 6 Strain, mm/mm profile along y–z section for 600 rpm and 60 mm/min



pin of the tool. Table 2 shows the experimental validation of the model with the maximum temperature data obtained from literature [19]. Maximum temperature obtained during the process is compared with the simulation results and the model is accurately able to predict it with a maximum error of 5.4 %.

Strain Profile

Plastic deformation of material plays a vital role in material movement and hence in formation of good weld. It also affects the microstructure of the weld zone along with thermal history. Therefore, it is important to study the strain distribution to understand the deformation of the material. Figure 4 shows the effective strain distribution in transverse direction of the weld for a rotational speed of 1000 rpm and a traverse speed of 60 mm/min.

Figure 5 clearly depicts that strain is higher on the top surface of the material as compared to the bottom. This is due to the fact that rotating shoulder contributes to the deformation of material more than the pin. Figure 6 shows the contour plot for 600 rpm rotational speed. Maximum

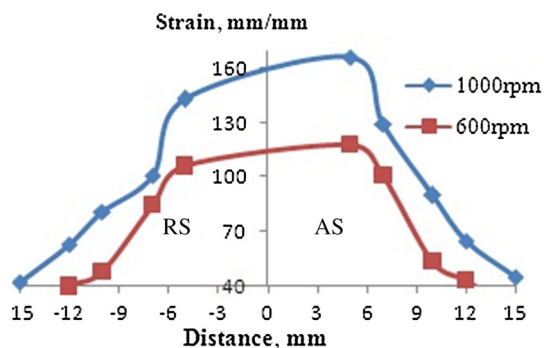


Fig. 7 Strain variations in FSW as a function of rotational speed

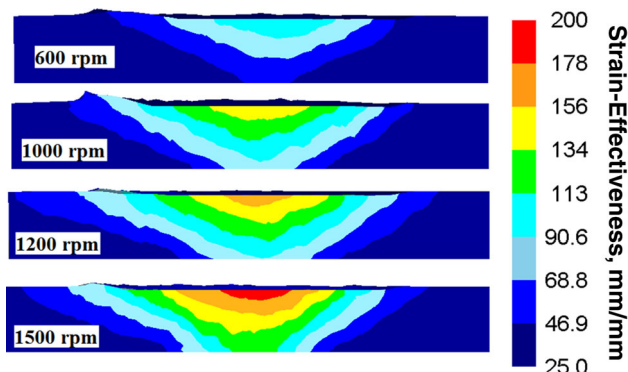


Fig. 8 Effect of rotational speed on plastic strain distribution for 60 mm/min welding speed

strain value is reduced due to reduction in rotational speed which leads to reduced deformation of the material. Figure 7 clearly indicates that strain in the Advancing Side (AS) of the welding is higher as compared to the Retreating Side (RS). This proves the asymmetric nature of the friction stir welding process. Higher strain on ‘AS’ as compared to that of ‘RS’ is due to positive impact of rotational and traverse velocities of the tool. Similar pattern is obtained for 600 rpm, but the values are reduced.

Figure 8 shows the effect of rotational speed on effective strain distribution along transverse direction for welding speed of 60 mm/min. It is clearly evident that with increase in rotational speed, effective strain increases. This is due to the fact that with an increase in the rotational speed of the tool, rotation per second of the tool increases, which in turn increases the deformation and hence increases strain. Also, with increase in rotational speed, width of the nugget zone increases and the same observation has been found experimentally [20].

Effect of welding speed on effective strain for a tool rotational speed of 1000 rpm is shown in Fig. 9 in the form of contour plot. Increase in the welding speed reduces the effective strain. This is due to the fact that with increase in

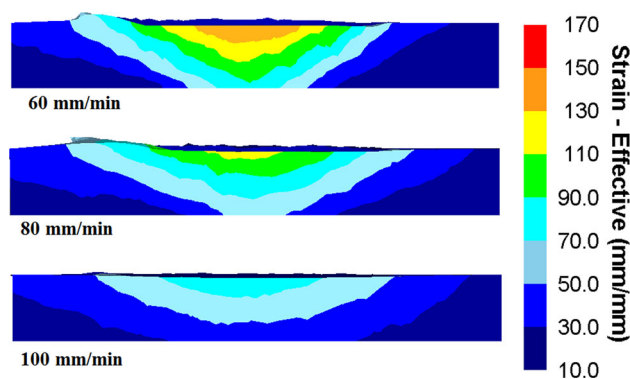


Fig. 9 Effect of welding speed on strain distribution for rotational speed of 1000 rpm

welding speed, time for deformation and heating reduces, which reduces the deformation during the process.

Conclusion

A 3D fully coupled temperature-displacement analysis is developed based on Lagrangian implicit method to understand the thermo-mechanical process of FSW process for AA2024 aluminum alloy. Model is capable of predicting temperature, strain, stress and other parameters which give insight into the FSW process. Effect of rotational speed and welding speed on plastic strain is studied. Maximum temperature of 546 °C is attained in the nugget zone, and the temperature profile attains a ‘V’ shape due to higher heat generation on the top surface as compared to the bottom. Higher strain is observed on the top surface of the work piece as compared to the bottom surface. Deformation increases with increase in rotational speed of the tool indicating higher strain, while it decreases with increase in welding speed. Strain distribution forms an inverted trapezoidal shape indicating the nugget zone of the process, which is formed due to stirring action of the pin. Strain distribution is not uniform which indicates asymmetrical nature of FSW process.

Acknowledgments This paper is a revised and expanded version of an article entitled, “Finite Element Simulation of Temperature and Strain Distribution in Al2024 Aluminum Alloy by Friction Stir Welding” presented in ‘5th International & 26th All India Manufacturing Technology, Design and Research Conference’, held at ‘Indian Institute of Technology Guwahati’, Guwahati, India during December 12–14, 2014.

References

1. W.M. Thomas, “Patent_FrictionWelding_ThomasTWI.pdf,” (1995)
2. R.S. Mishra, Z.Y. Ma, Friction stir welding and processing. Mater. Sci. Eng. R Rep. **50**(1–2), 1–78 (2005)

3. R. Jain, K. Kumari, R.K. Kesharwani, S. Kumar, S.K. Pal, S.B. Singh, S.K. Panda, A.K. Samantaray, Friction stir welding: Scope and recent development, in *Modern manufacturing engineering*, ed. by J. Paulo Davim (Springer, Berlin, 2015), pp. 179–228
4. Y.J. Chao, X. Qi, W. Tang, Heat transfer in friction stir welding—experimental and numerical studies. *J. Manuf. Sci. Eng.* **125**(1), 138 (2003)
5. C.M. Chen, R. Kovacevic, Finite element modeling of friction stir welding—thermal and thermomechanical analysis. *Int. J. Mach. Tools Manuf* **43**(13), 1319–1326 (2003)
6. M. Yu, W.Y. Li, J.L. Li, Y.J. Chao, Modelling of entire friction stir welding process by explicit finite element method. *Mater. Sci. Technol.* **28**(7), 812–817 (2012)
7. H. Schmidt, J. Hattel, J. Wert, An analytical model for the heat generation in friction stir welding. *Model. Simul. Mater. Sci. Eng.* **12**, 143–157 (2004)
8. A. Arora, R. Nandan, A.P. Reynolds, T. DebRoy, Torque, power requirement and stir zone geometry in friction stir welding through modeling and experiments. *Scr. Mater.* **60**, 13–16 (2009)
9. A. Arora, Z. Zhang, A. De, T. DebRoy, Strains and strain rates during friction stir welding. *Scr. Mater.* **61**(9), 863–866 (2009)
10. G. Buffa, J. Hua, R. Shivpuri, L. Fratini, A continuum based fem model for friction stir welding—model development. *Mater. Sci. Eng., A* **419**(1–2), 389–396 (2006)
11. G. Buffa, J. Hua, R. Shivpuri, L. Fratini, Design of the friction stir welding tool using the continuum based FEM model. *Mater. Sci. Eng., A* **419**(1–2), 381–388 (2006)
12. Z. Zhang, H.W. Zhang, A fully coupled thermo-mechanical model of friction stir welding. *Int. J. Adv. Manuf. Technol.* **37**(3–4), 279–293 (2008)
13. K. Gök, M. Aydın, Investigations of friction stir welding process using finite element method. *Int. J. Adv. Manuf. Technol.* **68**(1–4), 775–780 (2013)
14. M. Assidi, L. Fourment, S. Guerdoux, T. Nelson, Friction model for friction stir welding process simulation: calibrations from welding experiments. *Int. J. Mach. Tools Manuf* **50**(2), 143–155 (2010)
15. P. Asadi, R.A. Mahdavi, S. Tutunchilar, Simulation and experimental investigation of FSP of AZ91 magnesium alloy. *Mater. Sci. Eng., A* **528**(21), 6469–6477 (2011)
16. F. Al-Badour, N. Merah, A. Shuaib, A. Bazoune, Coupled Eulerian Lagrangian finite element modeling of friction stir welding processes. *J. Mater. Process. Technol.* **213**(8), 1433–1439 (2013)
17. S. Kobayashi, S.-I. OH, T. Altan, *Metal forming and the finite element method, Oxford series.* (1989)
18. R. Nandan, G.G. Roy, T.J. Lienert, T. Debroy, Three-dimensional heat and material flow during friction stir welding of mild steel. *Acta Mater.* **55**(3), 883–895 (2007)
19. V. Malik, N. Sanjeev, H.S. Hebbar, S.V. Kailas, Time efficient simulations of plunge and dwell phase of FSW and its significance in FSSW. *Proc. Mater. Sci.* **5**, 630–639 (2014)
20. K. Elangovan, V. Balasubramanian, Influences of tool pin profile and tool shoulder diameter on the formation of friction stir processing zone in AA6061 aluminium alloy. *Mater. Des.* **29**(2), 362–373 (2008)